High accuracy Kerr effect measurement technique

D. P. Shelton
Department of Physics, University of Nevada, Las Vegas, Las Vegas, Nevada 89154

(Received 7 October 1992; accepted for publication 30 November 1992)

Apparatus and techniques are demonstrated which allow gas phase dc electro-optic Kerr effect measurements to be made with 0.1% absolute accuracy and nanoradian sensitivity. Measurements of the electric-field-induced birefringence of a gas are calibrated against a liquid Kerr cell, which is in turn calibrated absolutely *in situ*. Some of the problems addressed in this work are control of stray birefringence in order to obtain an extinction ratio below 10^{-10}, a simple method for calibration of space charge effects in the CS_2 reference Kerr cell, construction of electrodes with accurately calculable fields, and an investigation of the sources of systematic errors and drifts and means to eliminate them.

I. INTRODUCTION

Molecular properties such as the polarizability anisotropy, and the first and second hyperpolarizabilities of relevance to nonlinear optics, may be determined by means of measurements of the electric-field-induced birefringence (dc electro-optic Kerr effect) of a gas sample.[1–3] This method has been applied to a wide range of atoms and molecules, but until recently, the best absolute accuracy obtained in these measurements had been in the 5%–10% range.[4–7] Most recently, several groups have made very careful measurements of the dc Kerr effect in gases, with a stated absolute accuracy of $\pm 1.5\%$.[8,9] However, even in the most recent experiments, discrepancies much larger than the estimated error bars are still observed for Kerr effect measurements.[9] Therefore, one purpose of this work is to assess and understand the limitations on the attainable accuracy of gas phase dc Kerr effect measurements.

A number of interesting and important problems may be addressed by means of very accurate gas phase dc Kerr effect measurements. One such problem is the lack of accurate absolute experimental determinations of nonlinear optical susceptibilities. For this problem, the dc Kerr effect has a unique advantage since it is the only nonlinear optical experiment which is capable of absolute measurements with an accuracy much better than 10%. Another problem is to determine the size of the vibrational hyperpolarizabilities of molecules.[10] Kerr effect measurements of 1% accuracy combined with already existing results from other independent nonlinear optical experiments will allow one to derive reliable information about vibrational hyperpolarizabilities. The experimental apparatus for such studies should combine high accuracy, high sensitivity, and a wide wavelength range of operation.

In a dc Kerr effect experiment, molecular properties are determined from measurements of the change in the polarization of light propagating through a gas sample subjected to a transverse static electric field $\bar{E}$. The induced birefringence of the sample results in a relative phase shift or retardation between the two orthogonal polarization components of the incident light wave. The optical retardation φ due to the electric-field-induced birefringence of a low-density gas of centrosymmetric diatomic molecules, with number density ρ and sample length D, is given by

$$\varphi=(\pi\rho D/3\lambda_0\epsilon_0)(\gamma+\Delta\alpha^2/5kT)E^2, \quad (1)$$

where λ_0 is the light wavelength in vacuum, $\Delta\alpha$ is the polarizability anisotropy, and γ is the second hyperpolarizability of the molecule, all in SI units. Refinements of Eq. (1) to allow for other molecular symmetries, local field effects, quantum effects, and intermolecular interactions are well known but do not have a direct bearing on the design of the experimental apparatus.[1–3,11] Equation (1) indicates that φ will be of order 1 μrad and smaller for typical experimental conditions, and it is the small size of φ that is one of the strongest constraints on the experiment design. Design considerations and apparatus for Kerr effect measurements of shot-noise-limited sensitivity over a wide wavelength range have already been described.[12] The present work describes the refinements of experimental apparatus and techniques which allow one to obtain gas phase dc Kerr effect measurements of 0.1% accuracy as well.

II. MEASUREMENT AND CALIBRATION PRINCIPLES

The fundamental quantity which is to be measured in a dc Kerr effect experiment is the optical retardation φ due to the induced birefringence of the sample. In this section we will address the principles of the retardation measurement and indicate the other quantities to be measured in order to extract molecular property values from Kerr effect experiments.

The behavior of electo-optical systems employed to measure the optical retardation φ may be described in terms of the Jones matrix calculus for polarized light.[13–15] In the simplest system for measuring the retardation φ due to the Kerr effect, the Kerr cell is placed between perfect, crossed polarizers with the applied electric field in the Kerr cell oriented at 45° to the initial polarization direction (see Fig. 1). The optic axis of the induced birefringence is parallel to the applied field $\bar{E}$. The retardation φ may be determined from a measurement of the intensity of the laser beam transmitted through this sequence of three elements, where the transmitted intensity may be calibrated by observing the intensity change due to rotating the second polarizer (analyzer) away from the crossed position.

 0034-6748/93/040917-15$06.00

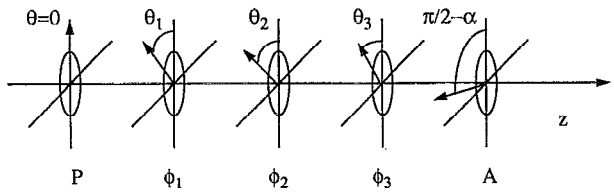

FIG. 1. A sequence of retardation plates between polarizers. A laser beam propagates along the z axis with its initial linear polarization defined by the first polarizer P. The polarization state of the light is modified as it passes through each retardation plate. The ith plate introduces a phase shift φ_i and is oriented with its optic axis at azimuthal angle θ_i. The final polarizer A (the "analyzer") transmits only that component which is linearly polarized polarized at angle $\pi/2-\alpha$. In the case that α and φ_i are all zero ("crossed" polarizers and no retarders), no light is transmitted ("extinction"). All azimuthal angles are measured with respect to the polarization direction of P. A retardation plate may represent a Kerr cell or some other birefringent element.

When the analyzer is uncrossed by an angle α, the transmitted intensity is given by

$$I/I_0=\sin^2\alpha+\cos(2\alpha)\sin^2(\varphi/2), \tag{2}$$

where I_0 is the incident intensity. A method for determining the retardation φ in terms of the rotation angle α, without photometric calibration difficulties, is to match the transmitted intensity with the Kerr cell on and the analyzer crossed, against the transmitted intensity with the Kerr cell off and the analyzer uncrossed. The intensity matching condition will be satisfied at two uncrossed angular positions of the analyzer: in the ideal case $\alpha_\pm=\pm\alpha^*$, where $2\alpha^*=\varphi^*$. The intensity-matching method for measuring φ^* is summarized by

$$\begin{aligned} &I(\varphi=\varphi^*,\alpha=0)=I(\varphi=0,\alpha=\alpha_\pm)\\ &\quad\rightarrow|\alpha_+-\alpha_-|=|\varphi^*|. \end{aligned} \tag{3}$$

Note that this method is unaffected by the addition of a constant background term to the detector output signal. Since the crossed position $\alpha_\times$ is relatively poorly defined because $dI/d\alpha=0$ at $\alpha=0$, it is preferable to measure $(\alpha_+-\alpha_-)$ rather than $2(\alpha_+-\alpha_\times)$. This method works well for $\varphi\gtrsim 10$ mrad, but several practical limitations make this method unsuitable for the measurement of small φ. Low sensitivity due to quadratic dependence on φ is one of the main limitations: $I/I_0\approx 10^{-13}$ for $\varphi\approx 1$ μrad.

The sensitivity limitations in the measurement of φ can be removed by employing heterodyne, modulation, and phase-sensitive detection techniques to obtain a signal which is linear in φ and to extract this signal from the background.[12,16] A minimal optical system for measuring the small retardation due to the Kerr effect in a gas consists of a gas Kerr cell (GKC) and a liquid Kerr cell (LKC) placed between crossed polarizers, with the applied electric fields oriented at 45° to the incident polarization. Applying a voltage $V=[V^{(0)}+V^{(\omega)}\cos\omega t]$ to a Kerr cell produces a retardation $\varphi=[\varphi^{(0)}+\varphi^{(\omega)}\cos\omega t+\varphi^{(2\omega)}\cos 2\omega t]$. For this system the amplitude of the component of the transmitted intensity oscillating at frequency ω is given by

$$I^{(\omega)}/I_0=\varphi^{(0)}\varphi^{(\omega)}/2, \tag{4}$$

where $\varphi^{(0)}$ and $\varphi^{(\omega)}$ are now the total retardances due to both Kerr cells. A large heterodyne magnification of the signal due to $\varphi^{(\omega)}$ is obtained when $\varphi^{(0)}\gg\varphi^{(\omega)}$. In the case that $\varphi^{(0)}=\varphi_L^{(0)}=20$ mrad is induced in the liquid Kerr cell and $\varphi^{(\omega)}=\varphi_G^{(\omega)}=1$ μrad is induced in the gas Kerr cell ($\varphi_G^{(0)}\approx 1$ μrad may be neglected), the intensity modulation will have an amplitude $I_G^{(\omega)}/I_0=10^{-8}$. The signal component $I_G^{(\omega)}$ is easily isolated using a lock-in amplifier tuned to the frequency and phase of the applied voltage modulation, and the signal $I_G^{(\omega)}$ is essentially background-free, linear in $\varphi_G^{(\omega)}$, and relatively large.

The liquid Kerr cell serves two purposes. First it serves as a convenient and controllable device for generating the large bias retardation $\varphi^{(0)}$ which is needed to obtain an easily measurable signal proportional to $\varphi_G^{(\omega)}$. Second, it provides a means to calibrate the gas Kerr signal by comparison. Modulating the voltage on the liquid Kerr cell rather than the gas Kerr cell generates a retardation $\varphi_L^{(\omega)}$ and a corresponding signal $I_L^{(\omega)}$, and the relation

$$\varphi_G^{(\omega)}=[I_G^{(\omega)}/I_L^{(\omega)}]\varphi_L^{(\omega)}, \tag{5}$$

then serves to calibrate $\varphi_G^{(\omega)}$ in terms of $\varphi_L^{(\omega)}$. In order to determine $\varphi_L^{(\omega)}$ one uses the following relations:

$$\varphi_L^{(0)}=K_L[F_L V_L^{(0)}]^2 \tag{6}$$

and

$$\varphi_L^{(\omega)}=2K_L F_L V_L^{(0)} V_L^{(\omega)}, \tag{7}$$

where K_L is the Kerr constant of the liquid cell in the absence of space charges and F_L is a factor which accounts for the space charge distortion of the field in the liquid. The retardation $\varphi_L^{(0)}$ is large enough to be measured by the method outlined in Eq. (3), and the Kerr constant K_L may be obtained from Eq. (6) [the factor $F_L\approx 1$ will be discussed later; see Eq. (16)]. The value of $\varphi_L^{(\omega)}$ may then be determined by means of Eq. (7).

The intrinsic molecular properties $\Delta\alpha$ and γ in Eq. (1) may be expressed in terms of directly measurable quantities by the relation

$$[\gamma+\Delta\alpha^2/5kT]=\left[\frac{3\epsilon_0\lambda_0 d^2}{\pi\rho D}\right]F_L K_L\left[\frac{V_L^{(0)}V_L^{(\omega)}}{V_G^{(0)}V_G^{(\omega)}}\right]\left[\frac{I_G^{(\omega)}}{I_L^{(\omega)}}\right], \tag{8}$$

where d is the spacing between the plane parallel electrodes of (effective) length D in the gas Kerr cell. The complete set of measurements includes a determination of the ratio of signal intensities $I^{(\omega)}$ employing a phase sensitive amplifier, measurement of the ratio of voltages applied to the Kerr cells, an absolute determination of the Kerr constant of the reference Kerr cell, and absolute determinations of sample density and gas Kerr cell electrode geometry. The treatment to this point has been for an ideal apparatus. In the next sections the effects of deviations from the ideal will be considered, and the important aspects which must be addressed in order to obtain accurate results in practice will be identified.

III. SYSTEMATIC ERROR ANALYSIS FOR RETARDATION MEASUREMENTS

In order to describe the real optical system one must also include the effects of small imperfections such as "stray" birefringence, misalignment, and scattering in optical components such as cell windows and polarizers. In the case that the optical components between the nearly crossed polarizers may be represented as a sequence of weak retardation plates, with retardations φ_i and axes oriented at arbitrary azimuthal angles θ_i with respect to the polarization direction of the first polarizer (see Fig. 1), then the lowest order approximation for the transmitted intensity is[13]

$$I/I_0=[\alpha]^2+[\Sigma_i(\varphi_i/2)\sin(2\theta_i)]^2+[S], \tag{9}$$

where the term S has been appended to describe the depolarized scattered light reaching the detector.

Consider the implications of Eq. (9) for the simple, absolute method for measuring φ that is outlined by Eq. (3). The first consequence of Eq. (9) is that even small imperfections in the optics render the method of Eq. (3) too insensitive to measure small retardations $\varphi_0 \approx 1$ μrad, since the small signal due to φ_0 will be buried in an overwhelmingly stronger background due to stray birefringence and scattering. The sensitivity limit for this method of measuring φ_0 is approximately set by the transmission I/I_0 observed with crossed polarizers and $\varphi_0=0$, the so-called "extinction ratio." The second consequence of Eq. (9) is that even when φ_0 to be measured is relatively large, such as during calibration of the LKC, stray retardations φ_i ($i\neq 0$) can introduce significant systematic errors. Suppose $\varphi_0=20$ mrad is to be measured with apparatus having an extinction ratio 10^{-6}. If the nonzero extinction ratio is due to scattered light only, the method of Eq. (3) will give exactly the correct result, but if imperfect extinction is due to stray retardations, the result will be in error by $\pm 10\%$. This is because stray retardations add to φ_0 "coherently" rather than in quadrature. In order to correctly account for the imperfections of the apparatus, not only must one distinguish scattering from stray retardation, but the transverse variation of the retardation must be assessed as well. In the absence of such detailed information, the extinction ratio of the apparatus would have to be below 10^{-10} to ensure that the measurement error is less than 0.1% for $\varphi_0=20$ mrad. In the case that the retardation of each element is small and uniform, Eq. (9) indicates how to minimize the effects of the stray retarders. Where possible, the fast or slow axis of an optical element should be oriented parallel to the incident polarization to minimize $(\varphi_i/2)\sin(2\theta_i)$ for that element. The residual effect of the stray retarders can be made to vanish by a fine adjustment of θ_i for one of the elements, such that $(\varphi_i/2)\sin(2\theta_i)$ for this element compensates the residual effect of all the others.

The discussion in the previous paragraph is based on Eq. (9), which is the lowest order approximation for I/I_0. Higher order terms must also be considered. The exact result for the transmitted intensity for a system of three arbitrary retarders placed between a pair of polarizers is presented in the Appendix. From that result one may show that applying the intensity-matching method of Eq. (3) to calibrate the liquid Kerr cell (LKC) gives

$$(\alpha_+-\alpha_-)=\varphi_L^{(0)}\sin 2\theta_L\left\{1+\phi/\varphi_L+\frac{1}{2}\varphi_{13}^2\sin^2 2\theta_{13}\right.$$
$$\left.-\frac{1}{4}\varphi_{13}^2\sin 2\theta_{13}\sin 2\Delta_L+\ldots\right\}, \tag{10}$$

where

$$\phi=(\varphi_1\sin 2\theta_1+\varphi_3\sin 2\theta_3), \tag{11}$$

φ_L is the retardation of the LKC oriented at θ_L (where $\Delta_L=\theta_L-\pi/4$ is small), and placed between stray retarders 1 and 3. Equation (10) has been simplified by using upper bounds for some of the correction terms, hence $\varphi_{13}=\max(|\varphi_1|,|\varphi_3|)$ and $\theta_{13}=\max(|\theta_1|,|\theta_3|)$. For $\varphi_{13}=3$ mrad and $\sin 2\theta_{13}=0.1$, the contribution due to all the correction terms beyond ϕ/φ_L is less than 10^{-7}. Note that ϕ may have either sign, so the term ϕ/φ_L will average to zero in the long run if the residual stray retardation remaining after compensation varies randomly about zero.

If the stray retardation is not uniform, then it will not be possible to achieve perfect compensation by simply reorienting one of the elements. The measured signal will be related to $\langle I(x,y)\rangle/\langle I_0(x,y)\rangle$, which may be expressed as the integrated product of the intensity transmission function and the normalized incident light intensity distribution. The main effect of this averaging will be to replace ϕ in Eq. (10) by $\langle\phi\rangle$. The dominant systematic error term in the calibration can still be made to vanish by compensating to obtain $\langle\phi\rangle=0$. However, in practice the compensation point is determined by minimizing the extinction ratio of the apparatus, which minimizes $\langle\phi^2\rangle$ and not $|\langle\phi\rangle|^2$. To assess the effect of nonuniform retardation, two types of variation will be considered: (i) birefringence with fixed orientation of the optic axis, but magnitude varying linearly in the x direction, and (ii) birefringence with radially directed optic axis and magnitude varying as r^2, where r is the distance from the symmetry axis of the optical component. The laser beam is assumed to be centered on the symmetry axis, and the incident light intensity distribution is assumed to be that of a Gaussian laser mode with beam diameter $2w$ (w is the radius at which the intensity falls to $1/e^2$ of the central intensity). The form of ϕ is

$$\phi=[a+b(x/w)]\sin 2\theta+c(r/w)^2\sin 2(\theta+\chi-\psi), \tag{12}$$

where the origin lies on the symmetry axis of the component, and transverse position in the optical component is specified by either Cartesian (x,y) or polar (r,ψ) coordinates. Measured with respect to the space-fixed direction defined by the polarization axis of the first polarizer (see Fig. 1), θ is the azimuthal angle of the optic axis of the linear term of ϕ, and $\theta+\chi-\psi$ is the azimuthal angle of the optic axis of the quadratic term of ϕ at position (r,ψ). This is the form one would expect for the birefringence of an axisymmetric optical element fabricated from nearly uniform material. A radial quadratic term could result from

residual strains after a cylinder of optical glass is annealed, or from strains due to thermal expansivity mismatch between an antireflection coating and the substrate, or from the radial stress distribution for a cell window under pressure.[17] The results of evaluating $\langle\phi\rangle$ and $\langle\phi^2\rangle$ for $\phi(x,y)$ given by Eq. (12) are

$$\langle\phi\rangle = a \sin 2\theta, \tag{13}$$

$$\langle\phi^2\rangle = a^2 \sin^2 2\theta + b^2 \sin^2 2\theta + 4c^2. \tag{14}$$

Therefore the desired condition $\langle\phi\rangle = 0$ is obtained, for the stray retardation specified by Eq. (12), when the extinction ratio $\langle\phi^2\rangle$ is minimized by compensation employing a uniform retarder. As a consequence, the systematic error in the LKC calibration will vanish; this is essentially due to symmetry. Note that the transmitted intensity distributions due to the a and c terms of Eq. (14) have little spatial overlap: 63% of the transmitted power lies inside $r/w = 1$ for the former but 92% lies outside $r/w = 1$ for the latter. This allows the terms in Eq. (14) to be experimentally distinguished. Equation (12), which leads to Eqs. (13) and (14), will be an adequate representation provided that the optical components are selected so that the birefringence is small and smooth on the scale of the beam diameter, the laser beam is aligned on the symmetry axis of each component, and the laser beam is narrow. The importance of a narrow beam to obtain the lowest extinction ratio has been previously noted.[18]

One may also use the expressions in the Appendix to analyze the calibration of the GKC signal, by comparison with the LKC signal, using the modulation and phase-sensitive detection method outlined in Sec. II. In the case that a stray retardance δ oriented at angle 2θ is interposed between the GKC and the LKC, the condition for matching $I_G^{(\omega)} = I_L^{(\omega)}$ becomes

$$\frac{\varphi_G^{(\omega)} \sin 2\theta_G}{\varphi_L^{(\omega)} \sin 2\theta_L} = 1 + \frac{1}{2} \frac{\delta^2 \cos^2 2\theta - \delta \cos 2\theta (\varphi_L^{(0)} - \delta \sin 2\theta) \sin 2\Delta_L}{1 + \delta \sin 2\theta / \varphi_L^{(0)}}, \tag{15}$$

where $\Delta_L = \theta_L - \pi/4$ is the misorientation of the LKC. The simultaneous presence of a small retardance $\varphi_G^{(0)}$ in addition to $\varphi_L^{(0)}$ introduces a negligible contribution to the systematic error. A small error in the orientation of the LKC has only a weak effect on the calibration of the GKC because the leading $\sin 2\theta_L$ factor also appears in the calibration equation for the LKC given by Eq. (10), and so it cancels out in the final analysis. In Eq. (15) the systematic error is controlled by δ, rather than by $\delta \sin 2\theta$ as in Eq. (10). In general, δ will not vanish, but the δ_i for a sequence of retarders may be made to partly cancel. The value of δ due to a pair of stray retarders can be minimized by orienting the fast axis of one parallel to the slow axis of the second; the same idea applies when δ is due to a sequence of several stray retarders, but then there are more combinations of retarder orientations to consider. For $\varphi_L^{(0)} = 20$ mrad, $\delta = 3$ mrad and $\sin(2\theta_L - \pi/2) = 0.1$, the systematic error will be less than 0.001%. The systematic error is the same for "comparison" and "compensation" methods of measurement ($\varphi_G^{(\omega)} = \pm\varphi_L^{(\omega)}$). Note that calibration can be performed *in situ*: the apparatus and operating conditions are exactly the same for calibration and measurement.

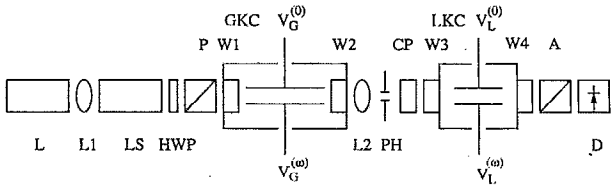

FIG. 2. Schematic diagram of the optical apparatus for Kerr effect measurements. The beam from a laser L is collimated by a lens $L1$ and intensity stabilized by an electro-optic light stabilizer LS. A half-wave retardation plate HWP is used to rotate the plane of polarization to 45° from the vertical to match the orientation of the polarizer P. The gas Kerr cell GKC is followed by a collimating lens $L2$, a 1-mm pinhole PH, a compensating plate CP, the reference liquid Kerr cell LKC, the analyzing polarizer A, and finally a 2.5 mm×2.5 mm Si photodiode detector D operating at zero bias at the input of a current-to-voltage amplifier. Both CP and the Kerr cell windows $W1$–$W4$ are Schott SF-57 zero-stress-birefringence glass. The plane-parallel electrodes of the GKC and LKC are separated by 3.2-mm ceramic spacers and are 46- and 10-cm long, respectively. The electrodes of both the GKC and the LKC are oriented vertically (field lines horizontal). At $\lambda_0 = 633$ nm the Kerr constants of the cells are approximately $K_G = 20$ nrad/kV^2 for the GKC filled with H_2 at 1 atm (7 μrad/kV^2 for CO_2 at 10 atm) and $K_L = 2$ mrad/kV^2 for the LKC filled with CS_2. Typical applied voltages are 5 kV and 200 V_{rms} for the GKC, and 3 kV and 20 mV_{rms} for the LKC. The apparatus is 3.5-m long overall, with 1.5 m between the crossed polarizers and 0.5 m from the analyzer to the detector. Lenses with focal length about 0.5 m are needed to maintain a diffraction limited beam diameter of 0.5 mm in the apparatus.

IV. EXPERIMENTAL APPARATUS: OPTICS

A schematic diagram of the apparatus is shown in Fig. 2. The design is dictated by the results of the previous section. The same optical configuration is used for GKC measurement and LKC calibration. The output beam of a laser (He-Ne, argon-ion, or dye laser) is collimated by a lens and passes through an electro-optic light stabilizer (CRI LS100) which stabilizes the average light power (0.05% long term) and reduces the optical noise (100 ×reduction at 2 kHz). With most lasers, this laser-noise reduction is needed to achieve sensitivity near the shot-noise limit.[12] Stabilized incident light power is also desirable since accurate retardation measurements and calibrations by means of photometric comparisons are difficult unless light intensity drifts and fluctuations are small.

Even though the input intensity is stabilized, vignetting apertures or transmission nonuniformities will transform small beam position variations into signal fluctuations and drifts. The most important source of signal drift in the present apparatus arises because the transmission of the windows is temperature dependent and nonuniform. This is the result of interference between the front-surface and back-surface reflections for each window. The window transmission is modulated on a millimeter spatial scale as a result of the typical 1-arcmin deviation from parallelism of

the window surfaces. The laser beam in the apparatus has a diameter of about 0.5 mm; this improves the extinction ratio but makes the beam transmission sensitive to the beam position relative to the interference fringe pattern. Furthermore, even when the beam does not move, there will be transmission drifts because the interference fringe pattern will shift over a whole fringe for a window temperature change of just a few °C. The transmission variations are adequately reduced by antireflection coatings, except in the LKC, where contact with the high refractive index liquid CS_2 renders the antireflection coatings ineffective and results in transmission variations of several percent. Signal drifts and fluctuations are reduced by temperature stabilizing the LKC, and the sequence of measurements is chosen such that the effects of drifts will tend to cancel.

The angular orientations of the analyzer and the GKC must be accurately determined to achieve 0.1% calibration accuracy. The analyzing polarizer is mounted on a precision sine-drive rotation stage (Oriel 13025). The smallest graduation of the drive micrometer corresponds to 0.0005°, and the calibration factor of the rotator has been checked to 0.02% against a precision divided circle. In a typical setup using a He-Ne gas laser ($\lambda_0=633$ nm), the laser beam power is 4 mW between the polarizers and a good operating point is obtained with a bias retardation $\varphi_L^{(0)}=18$ mrad produced by applying $V_L^{(0)}=3$ kV to the LKC. The LKC is calibrated at this operating point by means of the intensity-matching method of Eqs. (3) and (10). An accuracy of 0.0005° in the determination of the angle of rotation of the analyzer allows the 18 mrad retardation ($\alpha_+-\alpha_-=1°$) to be measured with better than 0.1% accuracy. The electric field in the GKC must be oriented at 45° to the incident light polarization direction. This is most easily accomplished by filling the GKC with CO_2 at several atmospheres pressure to obtain a conveniently large signal, and then rotating the GKC to maximize the ratio $I_G^{(\omega)}/I_L^{(\omega)}$. The typical orientation uncertainty of about ±0.5° gives a calibration error of 0.02%. The LKC does not need to be precisely oriented.

Equation (10) shows that stray retardation by the optical components introduces a systematic error into the calibration of the apparatus. Therefore, care must be taken to reduce stray birefringence. The critical components are those between the two polarizers. The polarizers are Glan-laser air-spaced calcite prism polarizers (Special Optics) with 10-mm aperture and broadband antireflection coatings on the entrance, exit, and side escape faces, and with uncoated central polarizing (Brewster's angle) surfaces. To achieve the lowest extinction ratio the best half of each polarizer should face inward (toward the Kerr cells). The windows of the GKC and the LKC are fabricated from zero-stress-birefringence glass (Schott SF-57 or Pockel's glass), 6-mm thick and 12.7-mm diameter, with plane-parallel, low-scatter surfaces antireflection coated with a $\lambda/4$ layer of MgF_2. The windows of the GKC are supported on plane-polished surfaces of the stainless-steel end plugs of the cell and are sealed with Viton O-rings. The end plugs have a central, 4-mm-diam aperture for the laser beam, and the windows are thick enough to support a pressure of 100 atm with little deformation.[17] The windows of the LKC are supported between Viton O-rings which also seal the cell. (The soft support of the LKC windows allows small tilt adjustments of each window with respect to the cell body; unless the entrance and exit windows are nearly parallel, the liquid filled cell will act as a prism, giving an undesirable temperature-dependent beam deflection.) As each window of each cell is installed, it is oriented so its stray birfringence axis is aligned with the incident polarization; this is the orientation which minimizes the light transmitted through the crossed analyzer. The compensator consists of one of these Pockel's glass windows on a rotation stage; ϕ of Eq. (11) may be compensated to zero with high sensitivity by making small angular adjustments to the azimuth of this window. The fused silica lens following the GKC is supported between O-rings and oriented to minimize the effect of residual birefringence; it is thermally isolated by enclosing it in a thick lucite shell since unshielded air drafts on the surface of the lens produce unacceptably large thermal-stress-induced birefringence fluctuations and drifts. The laser beam passes through the center of each of the optical elements. An aperture is introduced between the GKC and LKC to control scattered light which is reflected from the electrodes of the GKC.

The magnitude of the stray retardation and associated error may be estimated from the extinction ratio of the apparatus. The extinction ratio determined for the apparatus, set up as described above, is typically 3×10^{-8} (calibrated using the LKC), which in the worst case could indicate 0.4-mrad uncompensated stray retardance and 2% systematic errors. Therefore, it is important to understand the contributions to the measured extinction ratio. The stray retardation of the Pockel's glass windows was measured by scanning them through the laser beam between the crossed polarizers. The measured retardation distributions are smoothly varying and may be represented by a uniform retardation of about 3 mrad superimposed on a radially oriented contribution, quadratic in r, which increases by about 4 mrad going from center to edge of the window [$a\approx3$ mrad and $c\approx0.01$ mrad in Eq. (12), for a 0.5-mm-diam laser beam]. The signature of an uncompensated constant retardation term, which introduces a systematic error, will be a spot of light with the same profile as the incident beam. Based on the measured retardation of the windows, the extinction ratio of the complete apparatus with the constant retardation correctly compensated should be about 2×10^{-9}, with most of the transmitted light in the periphery of the beam. This prediction was tested by masking the photodiode with a pinhole whose diameter is equal to the laser beam diameter, and making a transverse scan with the masked detector assembly. The extinction ratio dropped to 2×10^{-9} and showed no peak at the beam position. A broad band of scattered light accounted for most of the detector signal, and the upper bound on the contribution to the extinction ratio due to an uncompensated constant retardation was 3×10^{-10}. To further test the performance of the compensator, the apparatus was stripped down so that only the LKC and the

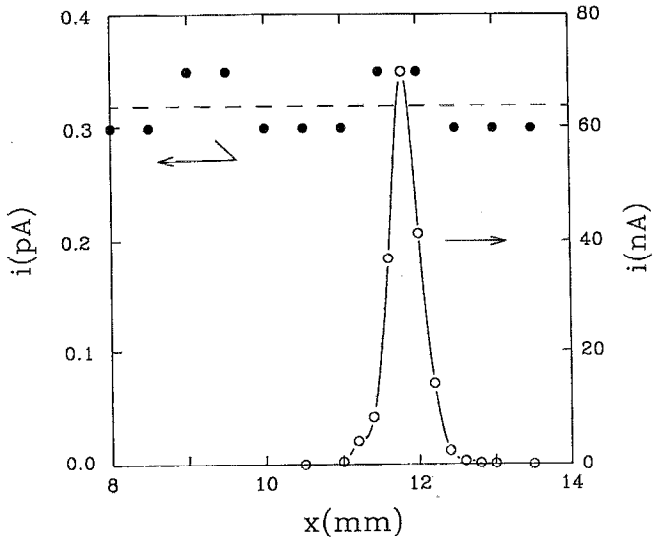

FIG. 3. Extinction ratio of the apparatus is determined by comparing the photodetector current with the LKC off (filled circles) to the current when $\varphi=18$ mrad is induced in the LKC (open circles). An extinction ratio 4×10^{-10} is estimated from the ratio of maximum photocurrents (the 25-pA diode dark current has been subtracted). The photodiode, masked by a 0.4-mm pinhole, was scanned across the beam position to map the spatial distribution of the light transmitted through the crossed polarizer in each case. A clearly defined beam spot is seen with the LKC on, but no significant spatial variation of the light is seen with the LKC off. Taking the upper bound on the intensity of the beam spot due to uncompensated retardation to be 10% of the apparently uniform background intensity due to scattered light (horizontal dashed line), the upper bound on the extinction ratio due to uncompensated retardation is 4×10^{-11}.

compensator plate remained between the crossed polarizers. Measuring the spatial distribution of transmitted light gives the results shown in Fig. 3. The extinction ratio including scattered light is 4×10^{-10}, but the contribution due to uncompensated retardation and having the same spatial profile as the laser beam is $<4\times10^{-11}$. Photographs of the light in the detector plane show a speckle pattern of scattered light and no trace of a transmitted beam, in agreement with the scanned-detector results. These observations demonstrate that compensation does indeed reduce $\langle\phi\rangle$ to the 10-μrad level or lower, as required for accurate calibration of the LKC. In the complete apparatus with the unmasked photodiode the extinction ratio is determined mainly by scattered light, with only a small stray retardation contribution from the $4c^2$ term of Eq. (14); neither contribution introduces a systematic error. The size of the small random retardation errors in setting the compensator can be estimated from the scatter of repeated LKC calibration measurements; the scatter of the calibration results is consistent with $\langle\phi\rangle$ less than 10 μrad and systematic calibration errors less than 0.05%.

V. SPACE CHARGE

The birefringence induced in the liquid CS_2 in the reference Kerr cell is due to molecular reorientation and relaxes on the picosecond time scale; for the present purpose the birefringence responds instantaneously to the applied field. The response of the liquid Kerr cell to the applied voltage is more complicated, with components which vary on the much longer time scale of 0.1–10 s. The time scale for calibration by the intensity-matching method of Eqs. (3) and (10) is several minutes, during which time the slow components will fully relax. However, when the liquid Kerr is employed to calibrate the gas Kerr cell measurements and the cell voltage is modulated at a frequency of $\nu\approx3$ kHz, the slow components of the LKC response will be unable to follow the modulation and the static calibration will not apply. The slow components of the response are due to distortion of the electric field in the LKC by space charges injected from the electrodes into the Kerr liquid. The effects of the space charge must be accounted for in order to obtain a valid calibration of the GKC measurements.

The LKC space charge effect can be assessed from a record of the transmitted intensity $I(t)$ following a voltage step from $V=0\rightarrow V=V_L^{(0)}$ at $t=0$. At $t=0$ the field in the homogenous insulating liquid between the plane-parallel electrodes will be $E_0=V_L^{(0)}/d$; redistribution or injection of charge carriers has not yet occurred. Later, at $t=\infty$, the steady-state space charge distribution will have been established and the field at the position of the laser beam will now be $E_\infty=F_L E_0$. Since $I\approx\varphi^2\approx E^4$, the factor by which the field has been modified due to the steady-state space charge distribution is simply determined from the ratio of final and initial transmitted intensities:

$$F_L=[I(t=\infty)/I(t=0)]^{1/4}. \tag{16}$$

Because the space charge distribution relaxes too slowly to respond to $V_L^{(\omega)}$, and provided that $V_L^{(\omega)}\ll V_L^{(0)}$ so that the time average of the injection current is not altered, the relation between the local value of the electric field in the liquid and the applied voltage is $E=d^{-1}(F_L V_L^{(0)}+V_L^{(\omega)})$. The effect of space charge is accounted for in Eqs. (6)–(8) by using the factor $F_L V_L^{(0)}$ rather than $V_L^{(0)}$. Note that the path of the laser beam through the LKC, and the applied voltage $V_L^{(0)}$, are the same in the LKC calibration, the GKC measurements and the F_L determination.

To allow an accurate measurement of $I(t=0)$, the voltage must step up to $V_L^{(0)}$ on a time scale short compared to the space charge relaxation time, and the voltage must remain constant to 0.01% during the $I(t)$ measurements. A high voltage step (3 kV) which relaxes to within 0.01% of the steady-state voltage within 20 ms is obtained by employing a stable, low-current (2.5 mA), stabilized high-voltage power supply (Bertan 205A-10R) followed by a simple mechanical switch (contact closing velocity of ≈1 m/s); the capacitance of the Kerr cell and the cable from the switch to the Kerr cell must be minimized (≈60 pF). To monitor the optical transient, the photocurrent from the detector is amplified by a simple transconductance amplifier (built from an LF 356 JFET operational amplifier) whose output signal will relax to within 0.01% of steady state in 3 ms. Figure 4(a) shows typical normalized $I(t)$ transients following 3-kV voltage steps; each trace gives the space charge distortion of the field at a

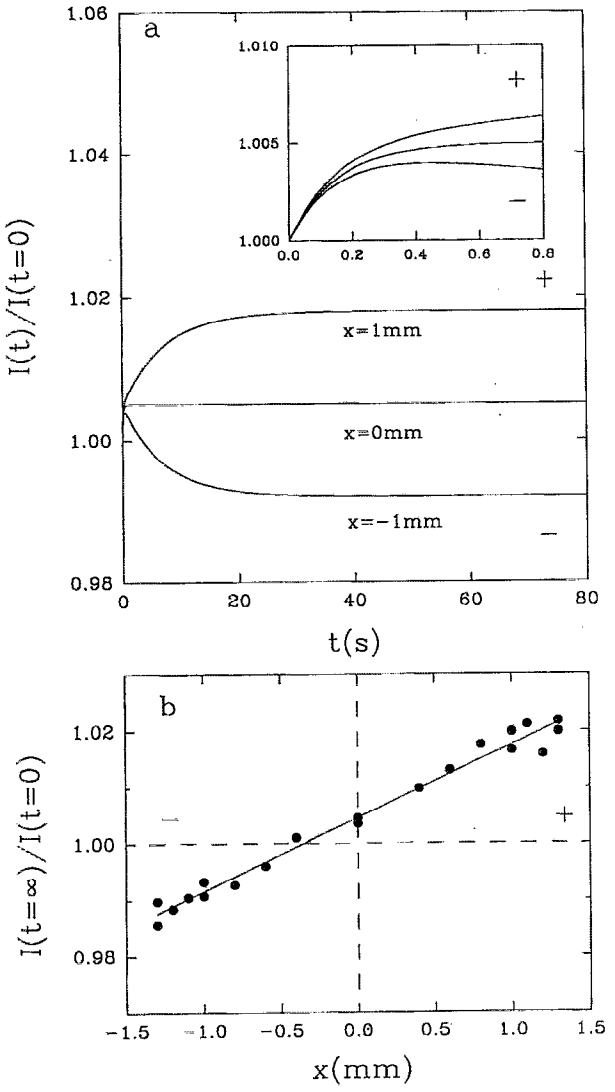

FIG. 4. The effect of space charge in the LKC is determined from the change in the transmitted light intensity following a step change in the voltage applied to the LKC ($V=0\rightarrow 3$ kV at $t=0$). (a) The normalized detected intensity $I(t)/I(t=0)$ is shown for three positions x of the laser beam with respect to the midplane of the LKC. The $+(-)$ electrode is at $+(-)$ 1.59 mm, and the laser beam diameter in the LKC is 0.5 mm. The slow intensity transient follows the production of the steady-state space charge distribution in the bulk of the liquid. The initial fast transient, shown in the inset with a 100× expanded time scale, is the same at all positions, and is consistent with the formation of a highly charged boundary layer 4-μm deep. (b) The linear increase of the ratio $I(t=\infty)/I(t=0)=F_L^4$ vs x as one moves from the $-$ to the $+$ electrode indicates a negative space charge of uniform density 70 μC/m^3 in the bulk of the CS_2. The space charge field correction factor F_L is determined with 0.05% accuracy. The LKC contained reagent grade CS_2 which had been dried over 3A molecular sieve and vacuum distilled into the LKC, giving a resistivity of 1×10^{12} Ω m (at $T=20$ °C).

different position in the LKC. Since the optical transmission varies across the face of the LKC, the intensity at $t=0$ is not independent of position in the LKC; the space charge distortion of the field cannot be reliably determined from the spatial variation of $I(t=\infty)$, whereas the ratio $I(t=\infty)/I(t=0)$ is a reliable measure. Figure 4(b) shows $I(t=\infty)/I(t=0)$ versus transverse position of the laser beam in the LKC, which is essentially a profile of the space charge field in the LKC. Near the midline of the LKC, the correction due to space charge is small and slowly varying.

Electric conduction and space charges in insulating liquids have been studied using potential probes and Kerr measurements.[19–22] The linear variation of the space charge field and the increase in the average field in the bulk of the LKC displayed by Fig. 4(b) disagrees with most other studies. However, diffusion controls the movement of the space charges in most other studies, either because low fields are applied or because injection at the electrodes is prevented (e.g., by electrodialysis with ion-selective membrane coated electrodes[22]). In the present case, with bare stainless-steel electrodes in contact with the liquid, homocharge injection may be expected (i.e., $+(-)$ charges injected at the $+(-)$ electrode). The applied field is large enough that the charged layer of dielectric near each electrode is convectively unstable, and the transport of space charge is mainly convective ("electroconvection," where the imbedded charges drag the fluid with them[23–26]). The space charge density in the bulk of the liquid is constant because of strong convective mixing, so the field increases linearly between the electrodes. The large space charge density due to injection into a thin unmixed boundary layer at the electrode surface reduces the field in this surface layer; almost the entire voltage drop occurs across the now somewhat thinner bulk region. The initial ($\tau\approx 150$ ms) upward transient in Fig. 4(a) is due to the rapid formation of the boundary layers by injection; as viewed by the bulk of the liquid between the electrodes, it appears as if the effective electrode surfaces have moved closer together. Subsequent transport and mixing of the injected charge into the bulk occurs over a longer time scale ($\tau\approx 7$ s). The onset of electroconvection is accompanied by a small transient deflection of the laser beam (up to 1 mrad). Placing a small aperture in front of the detector converts this transient beam deflection into a large amplitude, complicated ("turbulent") but reproducible fluctuation in the detector signal. The electrical current in the LKC shows a strong fast initial transient followed by a slow approach to steady state; the time constants of the current transients agree with the optical observations and the current densities are consistent with theoretical predictions. Measurement of the LKC steady-state conductance as the applied voltage is increased shows an initial decrease in conductance versus voltage consistent with space charge limited current in a motionless dielectric. Above 500 V the cell conductance increases with voltage, consistent with increasingly strong convective charge transport; the transition to electroconvection at this relatively high voltage is consistent with weak charge injection at the electrodes.

A possible complication in this analysis is that the transient in $I(t)$ could be due to the slow orientational relaxation of traces of suspended dust or contaminants dissolved from the Teflon and Viton in contact with the CS_2 in the LKC. In that case F_L should be considered as a correction for the frequency dependence of K_L rather than a space charge distortion factor, and the factor F_L should then be removed from Eqs. (7) and (8). A significant contribution to the LKC response due to such a slow mac-

romolecular reorientation mechanism may be ruled out because the time scale is wrong and because it could not account for the observed electrical transients.

VI. ELECTRODE GEOMETRY AND FRINGING FIELDS

The effective length D of plane-parallel electrodes with length D_0, thickness h, and spacing d, is obtained from the integral of E^2 along the laser beam path through the sample,

$$D=\int (E/E_0)^2 dz, \tag{17}$$

where $E_0=V/d$ is the uniform field between a pair of infinite plane-parallel electrodes with spacing d. The D appearing in Eqs. (1) and (8) is the effective length defined by Eq. (17). The effective length along the midplane of plane-parallel electrodes of finite length but infinite width, immersed in an infinite medium, is given by an expression due to Chaumont:[27,28]

$$D=D_0+(d/\pi)[1+(h/d)\ln(1+d/h)]. \tag{18}$$

The actual electrodes differ from this ideal in several ways: the walls of the cell (at zero potential) are not infinitely far away, the electrodes are not infinitely wide, the electrode voltages are not symmetric about zero, the beam path may lie off the midplane, the edges are not perfectly sharp, the spacing may not be constant, and space charge may distort the field. As shown in Fig. 5, the actual GKC electrodes are rectangular steel bars 460.46-mm long, 25.4-mm wide, 12.2-mm thick, spaced 3.1751 mm apart (the "gap width"), and the electrode ends are 3–5 gap widths from the interior end faces of a steel gas cell with inside diameter 51 mm (all dimensions at $T=20$ °C). The effective length D has been investigated for boundary conditions close to the experimental boundary conditions by means of numerical and analytic solutions of the two-dimensional Laplace equation.[29–32]

One may show that the GKC electrodes are in effect infinitely wide, by considering the analytic solution for the semi-infinite parallel-plate capacitor.[29,31] Inside the capacitor the field E approaches the value E_0 very rapidly, the difference decreasing exponentially with distance from the edge. At a distance just two gap widths inside from the edge the difference has already fallen to $(E_0-E)=10^{-6}E_0$; the centerline of the electrodes is four gap widths from the edge [see Fig. 5(a)].

The effect of the proximity of the conducting wall of the gas cell is to reduce D below the value given by Eq. (18). Figure 5(b) shows the configuration of the conducting surfaces near the ends of the electrodes. The transverse field is obtained from the derivative of the numerical solution for the potential. The distance between the geometrical end and the effective end of the electrodes, δD, is calculated by subtracting the unit-step reference function η from the integrand of Eq. (17) and integrating along a line

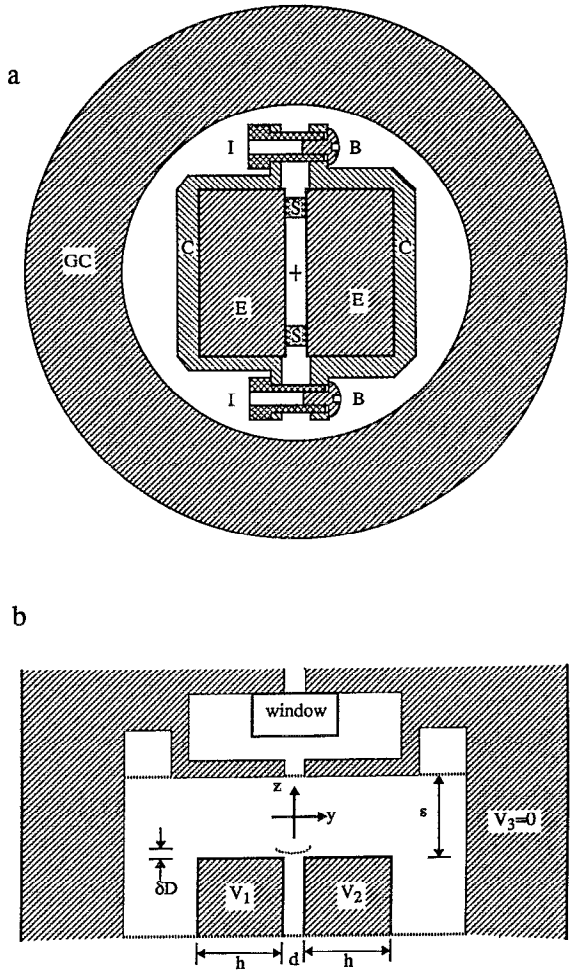

FIG. 5. (a) Cross-section through the electrode assembly at the position of one of the five sets of clamps and spacers. The polished steel electrodes E are pressed against ceramic gauge block spacers S by aluminum clamps C fastened together by a pair of bolts B and threaded Corning Macor ceramic insulating sleeves I. The corners and edges of the conductors are rounded and polished to avoid electrical breakdown (see text). The entire assembly is supported in the center of the cylindrical stainless-steel gas cell GC by two Macor ceramic blocks (not shown). The laser beam axis is shown by the cross. (b) Horizontal section showing the configuration of conducting surfaces near one end of the electrodes. The cell window is shielded from the fringing fields of the electrodes by a conducting cap. The position of the effective end of the field region (dotted curve), seen by a laser beam propagating parallel to the electrodes, depends on the thickness of the electrodes (in the present case $h/d=4$), the distance y of the beam from the midplane, the distance s between the grounded ($V_3=0$) window shield and the end of the electrodes, and the voltages V_1, V_2 applied to the electrodes. The fringing field was calculated numerically in 2D inside the rectangular region between the two dotted lines.

parallel to the midline of the electrodes and extending from the cell end-wall to a fiducial plane deep inside the interelectrode gap:

$$\delta D=\int [(E/E_0)^2-\eta]dz. \tag{19}$$

The value of δD is a function of the distance y between the beam path and the midline, the distance s from the electrodes to the end wall, and of the voltages V_1 and V_2

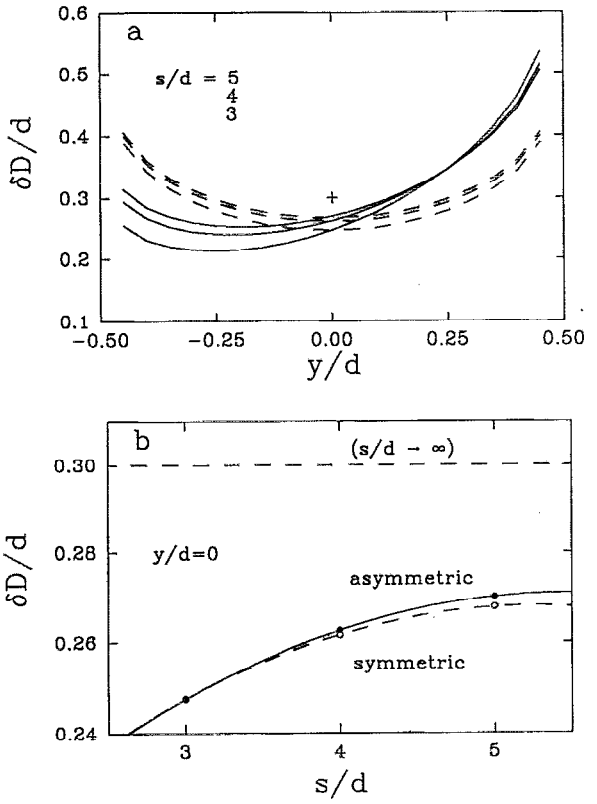

FIG. 6. (a) The distance between the effective end and the geometrical end of the electrodes, δD, is shown as a function of laser beam transverse position between the electrodes, for two voltage distributions and for several electrode to ground-plane distances s (the electrode separation is d, see Fig. 5). The fringing fields may be symmetric about the midplane (dashed line, $V_2=-V_1$), or asymmetric (solid line, $V_2=V$ at $+d/2$, $V_1=0$ at $-d/2$). The cross shows the effective length correction given by Eq. (18). (b) The effective length correction is shown as a function of s for a beam propagating along the midplane. The limit as $s\to\infty$ (horizontal dashed line) is given by Eq. (18). The effective length along the midplane is insensitive to the voltage distribution on the electrodes (solid curve, asymmetric fields; dashed curve, symmetric fields).

applied to electrodes 1 and 2 ($V_3=0$ for the cell wall). Results for $\delta D(y,s)$ are given in Fig. 6 for the symmetric ($V_2=-V_1$) and asymmetric ($V_1=0$) cases; the results for other voltage distributions will fall between these limiting cases. The apparatus is operated with large $V_G^{(0)}$ applied to one electrode and much smaller $V_G^{(\omega)}$ applied to the other, which corresponds to the asymmetric case. Note that δD is sensitive to small displacements of the beam path from the midline in this case. The presence of the conducting wall of the cell in our apparatus results in a fringing field correction about 10% smaller than that given by Eq. (18); the entire effective length correction due to the fringing field in the gas sample is about 0.4% of D_0. The SF-57 glass windows sealing the cell have a relatively large Kerr constant and must be shielded from the fringing fields of the electrodes. A metal enclosure surrounds each window and the flat circular end of this enclosure defines the end of the cell as seen by the electrodes. A small axial hole allows the laser beam to pass from the shielded enclosure into the electrode space, as shown in Fig. 5(b). With this arrangement, the transverse component of the fringing field on the axis at the window position is zero by symmetry.

The change δD_R in effective length due to rounding the sharp edges of the electrodes was also investigated. A rounded edge of radius R was approximated by a 45° bevel, $H\times H$, where $R\approx 1.7\ H$. The effect of replacing the sharp edges at one end of the electrodes by a small radius $R<d/10$ is to change the effective length of the electrodes along the midline by $\delta D_R\approx -0.20\ R$. The advantage of making R small is that this reduces the uncertainty in the effective length of the electrodes. The disadvantage of a sharp edge is that the electric field will be enhanced near the edge, so electrical breakdown of the gas sample will occur at a lower applied voltage and the maximum signal will be reduced. An electrode shape such as the Rogowski profile has the desirable property that the field nowhere exceeds the value E_0,[26] but electrodes with such a shape would be difficult to fabricate with the required precision. Rectangular electrodes with a small edge radius R joining the adjacent planar surfaces are a compromise between the demand for precise fabrication and the desire to maximize the attainable signal. The only edge radii which have a significant effect on the effective length D are those at the electrode edges on either side of the laser beam as it enters and leaves the gap between the electrodes. If these edges are sharp, one may show (for $h=\infty$) that the maximum field at a small distance R_e from the sharp 90° edge on one of the electrodes is[31]

$$E(R_e)=E_0(3\pi R_e/d)^{-1/3}. \tag{20}$$

The field diverges slowly, with $E<2E_0$ for $R_e>0.01d$, and $E<4E_0$ for $R_e>0.001d$. Equation (20) with $R_e\approx R_s+R$ may be used as an estimate of the maximum field strength at a distance R_s above the surface of the electrode with an edge of radius R. Since the enhanced field extends over only a short distance and then falls below E_0 (e.g., $E=E_0/\sqrt{2}$ at the midplane on the field line from edge to edge), the breakdown voltage will not be greatly reduced compared to a uniform field gap of the same width. Also, the peak field strength at the edges will be $<1/2$ the "corona" onset field,[26] for voltages up to the breakdown voltage in air at one atmosphere for all R in this geometry, so distortion of the fringing field by space charge will not be a problem (however, this result may depend on the particular gas surrounding the electrodes). To test these predictions, the breakdown voltage for electrodes with an edge radius of 10 μm was measured in air and compared to the value expected for a uniform field gap.[26] One finds that there is little penalty for sharp electrode edges in this geometry, as long as the corners where three edges meet are rounded: the measured breakdown voltage was 75% of the uniform field gap value, there was no observable corona, and breakdown actually occurred along the surfaces of the insulating spacers placed in the gap rather than at the electrode edges. The change in effective length D due rounding the electrode edges to a radius $R=10$ μm is -0.001% of D_0.

The geometrical factor d^2/D which characterizes the electrodes is most sensitive to small uncertainties in the interelectrode separation d; d must be known to 1 μm over the entire electrode surface to obtain 0.1% accuracy in d^2/D. To meet this requirement the electrodes consist of bars of 5% chromium tool steel ($L^{-1}dL/dT=1.2\times10^{-5}$/°C) whose surfaces have been lapped and polished flat. The gap width d is determined by five pairs of small spacers ($\sim9\times3\times3$ mm^3) placed at 10-cm intervals along the edges of the electrode bars. The spacers are cut from ceramic gauge blocks (Mitutoyo, $L^{-1}dL/dT=1.0\times10^{-5}$/°C) of partially stabilized zirconia.[33,34] The contacting surfaces are carefully cleaned, wrung together, and then lightly clamped at the position of each spacer [see Fig. 5(a)]. Since the electrodes will flex into contact with the spacers, the deviations from constant d for the assembly will be much smaller than the maximum deviation from absolute flatness along the length of each separate electrode, provided that the electrode surfaces are sufficiently regular in shape.

Sufficiently flat electrode surfaces were produced in two steps. First the electrode surfaces were fine ground on a large cast iron lapping plate. The surface profile of the lapping plate was adjusted by wear conditioning with a large ring tool, and surface flatness was determined from measurements of the thickness variation along the length of an electrode bar after both faces had been lapped to the same shape (taking care not to flex the bar). The maximum deviation of the fine ground electrode surfaces from flatness was 1 μm. Next, the electrode bars were placed parallel to each other with their critical faces against the lapping plate, glued to a rigid support, and lapped to make their critical surfaces coplanar and flat. Finally the critical faces were polished with an 8-in.-diam Buehler Metlap platen (which was lapped flat on the lapping plate) and 3-μm diamond suspension. After detaching the bars from the support, the less critical surfaces were polished with a smaller polisher, the critical inside edges at each end were left with a 5-μm radius, the other edges were beveled 0.1-mm wide, and the corners were rounded to a 1-mm radius. The electrode surface profiles were measured using interference fringes with an optical flat. In the narrow direction each surface is flat to better than 0.05 μm, while in the long direction each surface deviates in a smooth fashion by up to ±0.1 μm from a convex sphere about 0.5-μm deep. Based on the measured profile of each electrode surface, the deviations from constant d are estimated to be less than ±0.1 μm for the assembled electrodes. The estimated uncertainty in the effective spacing $\langle d^{-2}\rangle^{-1/2}$, due to roughness and irregularity of the electrodes and the uncertainty of the gauge block thickness calibration, is ±0.1 μm. As a check against gross errors, the gap width was determined from the difference between the thickness of the assembly and the sum of the thicknesses of the electrode bars, measured at 19 positions along the electrodes. The measured values of d fell within a 1-μm range, and the value $\langle d^{-2}\rangle^{-1/2}=3.174\pm0.003$ mm determined from these measurements agrees with the constructed dimension $d=3.1751\pm0.0001$ mm. As a final consideration, since zirconia ceramic is a very poor electrical insulator compared to silica or alumina,[33–35] heating of the spacers when high voltage is applied could significantly alter the gap width. However, the measured resistance of the ten spacers in parallel is 300 GΩ at room temperature, which is sufficiently high that heating is not a problem. The geometrical factor describing the electrode assembly was determined to be $d^2/D=2.1815\times10^{-5}$ m with an overall uncertainty of $\pm0.02\%$ (at 20 °C, for $s/d=4$). The contributions to this uncertainty, in order of decreasing size, come from the fringing fields, electrode spacing, and electrode length.

The design considerations for the Kerr cell electrodes are similar to those for the electrodes employed in high-field Stark spectroscopy,[36,37] with the added constraint that in the present case the fringing field at each end must also be accurately calculable. For Stark electrodes with construction and dimensions similar to ours, electrode spacing uniformity of 0.1 μm has been obtained as demonstrated by the observed spectroscopic linewidth. Absolute accuracy and long-term stability of 0.01% for the electric field has also been obtained, again tested spectroscopically. These results confirm that high geometrical accuracy is in fact attainable, and they also indicate that the usual careful cleaning of the electrode surfaces is sufficient to eliminate significant systematic errors that would result from charging of insulating surface layers.[38]

VII. ac VOLTAGE MEASUREMENT

There is no difficulty in measuring dc high voltages up to 10 kV with 0.01% absolute accuracy using a voltage divider and voltmeter (Fluke 80E-10 and 8842A/09), but high accuracy absolute ac voltage measurements are more difficult. To obtain accurate results employing Eq. (8) the ac voltages applied to the LKC and the GKC must have the same phase and the same waveform, but it is sufficient to determine just the ac voltage ratio $V_L^{(\omega)}/V_G^{(\omega)}$ rather than the absolute ac voltages. Since typically $V_L^{(\omega)}\ll V_G^{(\omega)}$, the measurement requirements may be satisfied by producing $V_L^{(\omega)}$ from $V_G^{(\omega)}$ using a suitable calibrated voltage divider.

Figure 7 shows the schematic diagram for such a voltage divider. Stable HVAC up to 500 $V_{\rm rms}$ at a frequency of 1–10 kHz is produced by amplifying the reference oscillator output signal from the lock-in amplifier and driving a ferrite core transformer (television "fly-back" transformer, resonant at about 40 kHz, off-resonance ratio $\approx17\times$). The HVAC is applied to the resistor-capacitor voltage divider through a blocking capacitor C_B. The effect of stray distributed capacitance on the top leg of the voltage divider is minimized by enclosing R_1 and C_1 in a metal shield held at $V_1/2$ by a simple resistive voltage divider.[26] The capacitive part of the divider is employed to allow the phase shifts due to cable, Kerr cell, and other capacitances to be compensated; at the typical operating frequency of 3 kHz the parameter $\omega R_1C_1=0.11$ and most of the current flows through the resistive divider. Metal film resistors are used in the divider for high stability and low reactance.[39] Low-temperature coefficient ceramic and polypropylene capaci-

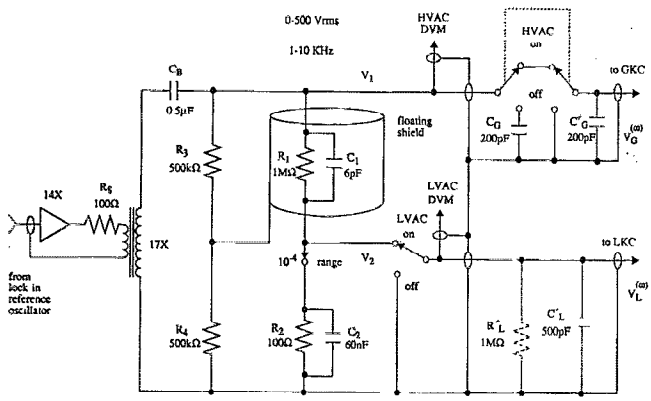

FIG. 7. Schematic diagram of the high voltage ac generator and ac voltage divider, which produces in-phase high and low voltage signals (HVAC$=V_1=V_G^{(\omega)}$ and LVAC$=V_2=V_L^{(\omega)}$). An audio frequency amplifier drives a transformer through a current limiting series resistance R_S (for overload protection at high and low frequencies), and the output of the transformer is applied to the voltage divider through a dc-blocking capacitor C_B (which allows the divider ratio to be calibrated by applying a dc high voltage to the HVAC output as discussed in the text). The voltage divider is composed of $R_1 \| C_1$ (R_1 in parallel with C_1) and $R_2 \| C_2$, where a separate pair $R_2 \| C_2$ is provided for each of the ten range switch settings (divider ratios 10^{-5}–10^{-2}, components for only one ratio shown). The output voltages are monitored by two digital voltmeters (DVM). Phase and amplitude errors due to stray distributed capacitance are minimized by enclosing $R_1 \| C_1$ in a cylindrical shield maintained at potential $V_1/2$ by the auxillary divider formed by R_3 and R_4 (Ref. 26). The dummy load C_G matches the total capacitive load C'_G following the HVAC switch, and is incorporated to ensure that the output amplitude and phase are independent of the HVAC switch position. The values of R_2 and C_2 are trimmed to allow for a total load on the LVAC output of 1 MΩ$\|$ 500 pF ($R'_L \| C'_L$).

tors are used. A switch selects R_2 and C_2 in the lower leg of the divider to give divider ratios ranging from 10^{-5} to 10^{-2} in ten steps.

The voltage ratio and phase shift for the divider formed by R_1, C_1, R_2, C_2 are given by

$$\left|\frac{V_2}{V_1}\right| = \left[\frac{R_2}{R_1+R_2}\right]\left[\frac{1+(\omega R_1 C_1)^2}{1+(\omega R_1 C_1)^2\kappa^2}\right]^{1/2} \tag{21}$$

and

$$\tan\theta = \frac{-(\omega R_1 C_1)(1-\kappa)}{1+(\omega R_1 C_1)^2\kappa}, \tag{22}$$

where

$$\kappa = \left[\frac{R_2}{R_1+R_2}\right]\left[\frac{C_1+C_2}{C_1}\right]. \tag{23}$$

The fractional mismatch of the resistive and capacitive divider ratios is given by $(1-\kappa)$. When $(1-\kappa)=0$ the phase shift between V_1 and V_2 is zero and the voltage divider ratio is the same for ac and dc voltages. If the resistive and capacitive dividers have been matched, then the ac voltage divider ratio may be calibrated by applying a dc voltage and measuring the divider ratio with a high impedance, high accuracy, dc voltmeter (even the thermal and voltage coefficient effects in the divider are the same if the dc voltage applied during calibration is equal to the rms ac voltage present during use of the divider). The resistive and capacitive dividers are matched by trimming the components to achieve zero phase shift between V_1 and V_2. The phase shift between V_1 and V_2 can be measured to 0.1° by applying these voltages to the Kerr cells and using the lock-in amplifier to measure the phase of the optical signal generated by the GKC and then by the LKC (filling the GKC with CO_2 gives a conveniently strong signal). In the case that both $(\omega R_1 C_1)$ and $(1-\kappa)$ are small, the voltage ratio and phase shift are $|V_2/V_1| \approx |V_2/V_1|_{dc} \times[1+(\omega R_1 C_1)^2(1-\kappa)]$ and $\theta \approx -(\omega R_1 C_1)(1-\kappa)$. The systematic error in the dc calibration of the ac voltage ratio at 3 kHz, for the divider in Fig. 7, will be 0.02% when the phase shift measured for the divider is 0.1°. As a check against gross errors, the ac voltage ratio was measured using two ac voltmeters (Fluke 8842A/09). The ±0.05% differences between the measured ac and dc voltage ratios (for ratios $> 10^{-4}$) are much smaller than the corresponding ±0.15% uncertainties due to the limited accuracy of our best absolute ac voltage measurements; the results are consistent with zero systematic error.

The Kerr effect measurements are made by alternately applying HVAC to the GKC, then LVAC to the LKC, and comparing the resulting optical signals ($V_L^{(0)}$ is fixed while $V_G^{(0)}$ is adjusted so that $I_L^{(\omega)}=I_G^{(\omega)}$ at the photodiode). For an accurate comparison, both the voltage divider ratio and the HVAC output voltage must be stable. For this reason, when the HVAC is disconnected from the GKC the switch also connects a capacitor to the HVAC output as a dummy load. This capacitor is trimmed so that the voltmeter monitoring the HVAC shows no change when the HVAC is switched from the GKC to the dummy load. Dummy load substitution is not needed at the LVAC output since the loading effect there is reduced by a factor equal to the divider ratio. However, since the the voltage divider ratio and phase shift are sensitive to the capacitive and resistive loading due to the monitoring voltmeter, the LKC and the cables connected to the LVAC output, the total external load must be trimmed to match the design load of the voltage divider. The voltage divider ratio is calibrated with all loads in place. The usual precautions of shielding and isolation from ground to break ground loops are incorporated into the voltage divider and HVAC source to prevent spurious signals due to pickup.[39] A sensitive test for possible systematic errors due to pickup is to set $V_G^{(0)}=0$ on the GKC and switch the HVAC to the GKC on and off; the lock-in amplifier output should not change.

VIII. COMPARISON WITH PREVIOUS WORK

Table I summarizes the apparatus previously used for gas phase Kerr effect measurements.[4–9] In all cases, the retardation induced in the GKC is made observable by a combination of modulation, heterodyne magnification and phase sensitive detection, and the GKC signal is measured by comparison ("match") or compensation ("null") using the signal produced in a previously calibrated reference cell. These principles are implemented in different ways in the different apparatus. In the present apparatus, the mod-

TABLE I. Comparison of present and previous gas phase Kerr effect measurement apparatus. The input laser beam passes through a sequence of the following optical elements between the polarizer (P) and analyzer (A): gas Kerr cell (GKC), liquid Kerr cell (LKC), compensator plate (CP), quarter wave plate (QWP), and Faraday rotator (FR). At least one of the applied fields is modulated at frequency ω, and the signal at ω or 2ω due to the GKC is measured by either comparing it to the signal produced by the reference cell (match) or by compensating it with the signal produced by the reference cell (null). The reference cell is either a LKC or a FR. The estimated uncertainty of measurements made with each apparatus is indicated.

Error	GKC	LKC	CP	QWP	FR	D	Reference
0.1%	ac+dc	ac+dc	yes	no	no	ω,match	Present work
1.5%	ac+dc	ac+dc	no	yes	no[a]	ω,null	Ritchie *et al.* (Ref. 8)
1.5%	dc	no	no	yes[b]	ac+dc	ω,null	Huttner *et al.* (Ref. 9)
3%	ac	no	yes	yes	ac	2ω,match[c]	Carusotto *et al.* (Ref. 7)
5%	dc	no	no	yes	ac+dc	ω,null	Buckingham *et al.* (Ref. 5)
5%	ac	ac	no	no	no	2ω,null	Burnham *et al.* (Ref. 6)
15%	ac	ac+dc	no	no[d]	no	2ω,null	Boyle *et al.* (Ref. 4)

[a]ac+dc FR used in calibration of LKC.
[b]dc FR calibrated with QWP removed.
[c]Several simultaneous modulation frequencies are employed.
[d]QWP used in LKC calibration.

ulated retardation $\varphi_G^{(\omega)}$ which is to be measured is proportional to the product of the ac and dc voltages applied to the GKC. This small modulated retardation is mixed with the much larger dc retardation $\varphi_L^{(0)}$ induced in the LKC by a large dc voltage, resulting in light intensity modulation at frequency ω which is measured with the lock-in amplifier. The signal is calibrated by comparing it to a nearly equal signal produced by applying a small ac voltage to the LKC (signal "match"). The LKC is itself calibrated in terms a mechanical rotation of the analyzer. Two disadvantages of this apparatus are that stray retardation must be carefully compensated and ac voltage measurements are required.

In the apparatus of Gentle *et al.*[8] the same large ac voltage is simultaneously applied to the LKC and GKC, thus avoiding the difficulties of ac voltage measurement. A large dc voltage is applied to the GKC to produce a retardation modulated at frequency ω, and a small dc voltage is applied to the LKC and adjusted so that the effects of the modulated retardations due to the GKC and LKC cancel (signal "null"). The null method is essentially equivalent to the match method when accurate photometric comparisons are possible, but the null method will have some advantage when the light intensity drifts or cannot be accurately measured. A major difference is that a quarter wave plate (QWP) at azimuth $\theta=0$ follows the Kerr cells and converts the incident elliptical polarization to a rotated linear polarization state in Ritchie's apparatus. With a QWP in the system, the transmitted light can be extinguished by orienting the analyzer at $\alpha=-\varphi/2$,[13,40] and rotating the analyzer is equivalent to inserting a retarder before the QWP. There are two important consequences. First, a static offset angle $2\alpha^{(0)}$ can serve instead of the static retardation $\varphi_L^{(0)}$ to produce the heterodyne enhancement of the optical signal $I^{(\omega)}$ (the dc retardation of the LKC may be too small to serve this purpose, since in this apparatus the LKC is filled with cyclohexane, which has a Kerr constant $50\times$ smaller than that of CS_2). Second, the LKC can be calibrated by applying a dc voltage and simply measuring the change in azimuth of the analyzer needed to regain extinction of the transmitted light. Actually, to increase the sensitivity, the analyzer is fixed and the plane of polarization is rotated through $\alpha^{(0)}$ with a Faraday rotator, and also, a second Faraday rotator is employed to modulate the plane of polarization with amplitude $\alpha^{(\omega)}$. This "vibrating analyzer polarimeter" employs modulation, heterodyne, and lock-in amplifier techniques but reverses the roles of the ac and dc terms: $\alpha^{(0)}$ is now the signal and $\alpha^{(\omega)}$ is the heterodyne background term. The LKC is calibrated against the dc Faraday rotator, which is in turn calibrated by a mechanical rotation of the analyzer.

An alternative means of eliminating ac voltage measurements is embodied in the apparatus of Tammer and Huttner,[9] and was before that employed by Buckingham and Sutter.[5] A large dc voltage is applied to the GKC and the static retardation induced in the GKC is measured by means of a "vibrating analyzer polarimeter" such as described above. In this apparatus the LKC is eliminated in favor of a Faraday rotator as the reference cell.

The apparatus of Carusotto *et al.*[7] is the most complicated, with four distinct modulation frequencies, two lock-in amplifiers, and a spectrum analyzer. The retardation modulated at 2ω due to the ac voltage applied to the GKC is compared, after elliptical to linear polarization conversion by a QWP, with the rotation produced by a Faraday rotator modulated at a nearby frequency. The remaining apparatus, that of Burnham *et al.*[6] and that of Boyle *et al.*,[4] also employs a GKC driven by an ac voltage only, but neither uses a QWP. In the former, stray birefringence provides the heterodyne background term, and the GKC signal is nulled by that from an ac LKC with electrodes at 90° to the GKC electrodes. In the latter, a dc LKC is used to produce the heterodyne background retardation, a second ac+dc LKC serves as the reference cell, and a frequency doubler is used to generate the ac voltage at 2ω needed to drive the reference LKC.

The absence of a QWP is the most notable difference between the present apparatus and all the other recently developed apparatus. The main advantages of employing a QWP as an elliptical-to-linear polarization converter are that measurement of φ becomes most direct, and measurement of φ becomes insensitive to stray retardation. The systematic errors due to stray birefringence in apparatus

including a QWP have been analyzed using the expressions given in the Appendix. One may show that in the comparison of $\varphi_G^{(\omega)}$ and $\varphi_L^{(\omega)}$, inserting a QWP has no effect on the systematic error due to a stray retarder intervening between the GKC and the LKC. Equation (15) still gives the result of a match or null measurement, except that the heterodyne background term $\varphi_L^{(0)}$ is replaced by $2\alpha^{(0)}$ if an analyzer angle offset rather than a bias retardation is employed. However, inserting a QWP will have a significant effect on the systematic error in the calibration of the LKC. Consider the case in which the retardance $\varphi_L^{(0)}$ induced in the LKC by an applied dc voltage is measured as the change in the analyzer angle, $\Delta(-2\alpha^{(0)})$, needed to restore extinction after the dc voltage is applied to the LKC. Assuming small misorientations and imperfections of the components and including the lowest order corrections, calibrating the LKC in this way gives

$$\Delta(-2\alpha^{(0)})=\varphi_L^{(0)}\sin 2\theta_L\left[1-\frac{1}{2}\delta_1^2\cos^2 2\theta_1-\frac{1}{2}\delta_2^2\right]\Big/ \cos 2\theta_Q, \tag{24}$$

where δ_1 is the stray retardance placed between the LKC and QWP, δ_2 is the stray retardance placed after the QWP, and θ_L and θ_Q are the azimuthal angles for the LKC and QWP. The signal-match method gives the same result as the signal-null method. For apparatus incorporating a QWP the leading calibration corrections due to stray birefringence are of order δ^2, in contrast to the leading zeroth order correction $\phi/\varphi_L^{(0)}$ appearing in Eq. (10) for the apparatus without the QWP. The systematic error is also second order in the QWP misorientation and retardance imperfection. The principal disadvantage of the QWP is that its retardance is usually strongly wavelength dependent so that operation of the apparatus is restricted to a narrow wavelength range. A second disadvantage is that since the signal $I^{(\omega)}$ during the GKC measurement is proportional to $2\alpha^{(0)}$, the apparatus with the QWP is more sensitive to mechanical disturbances; analyzer angle variations at the μrad level may be a significant source of noise and drift during (usually noise limited) GKC measurements even when the null method is employed.

The systematic errors which may limit the attainable accuracy of Kerr effect measurements will depend on choices taken in the design of the apparatus. One may identify four key aspects: the effect of stray retardation, transferability of the reference cell calibration, electrode geometry, and ac voltage measurement. The present work has shown how to deal with each of these sources of systematic errors in Kerr measurements. Section IV demonstrates effective procedures for eliminating systematic errors due to stray birefringence, even in the worst case of apparatus without a QWP. Section V shows how to avoid systematic errors due to space charge when a LKC is used as a reference cell. Section VI addresses the construction of Kerr electrodes with accurately calculable fields, and Sec. VII describes simple methods for accurate determination of ac voltage ratios. The analysis presented here indicates that the first three entries of Table I represent different optical configurations which should all be capable of Kerr effect measurements of the highest accuracy. In conclusion, absolute determinations of molecular property values with 0.1% accuracy appear to be feasible with only minor modifications of existing apparatus and procedures.

ACKNOWLEDGMENTS

This work was supported in part by a grant from the Research Corporation. The author wishes to thank Guo-Rong Fang and Heinz Knocke for help in constructing the electrodes, Terry Gibbons for help in preparing the manuscript, Bruce Rugar for help in characterizing the ac voltage divider, and Manson Wong for assistance in the fringing field calculations.

APPENDIX

The effect of a given system of polarizers, retarders, and rotators on a polarized light beam may be analyzed by means of the Jones calculus. The simplest optical system which is sufficient to represent all the types of Kerr effect measurement apparatus of interest in the present study is the sequence of three retarders between two polarizers, shown in Fig. 1. The effect of this system on the incident polarization state $\bar{\mathbf{v}}_0$ is represented in the Jones calculus by the expression[13]

$$\bar{\mathbf{v}}=\mathbf{P}(\pi/2-\alpha)\mathbf{J}(\varphi_3,\theta_3)\mathbf{J}(\varphi_2,\theta_2)\mathbf{J}(\varphi_1,\theta_1)\mathbf{P}(0)\bar{\mathbf{v}}_0, \tag{25}$$

where $\bar{\mathbf{v}}$ is the transmitted Jones vector, and $\mathbf{J}(\varphi,\theta)$ and $\mathbf{P}(\theta)$ are the matrices for the retarders and polarizers. The intensity of the light transmitted by the system is given by $I/I_0=|\bar{\mathbf{v}}|^2/|\bar{\mathbf{v}}_0|^2$. The three retarders in Eq. (25) can represent elements such as a Kerr cell, a quarter wave retardation plate, or a stray retarder due to window birefringence. The effect of a rotator $\mathbf{R}(\theta)$ placed before the analyzing polarizer is equivalent to rotating the analyzer by the same angle, so a Faraday rotator can also be implicitly represented. The angle α is the deviation of the analyzer from the crossed position.

The derivation of the results presented here will only be sketched. Equation (25) is most easily evaluated by representing the retarders as linear combinations of Pauli matrices, as described by Piazza *et al.*[13] Applying the product rules for the Pauli matrices greatly simplifies the calculation. The matrix **A** which represents the sequence of retarders may be written as

$$\mathbf{A}=A_1\mathbf{I}+A_2\mathbf{i}+A_3\mathbf{j}+A_4\mathbf{k}, \tag{26}$$

where **I**,**i**,**j**,**k** are the identity matrix and the three Pauli matrices, respectively. The transmitted intensity for the system is given by

$$I/I_0=\frac{1}{2}(1-\cos 2\alpha)+(A_3^2+A_4^2)\cos 2\alpha + (A_2A_4-A_1A_3)\sin 2\alpha. \tag{27}$$

From the coefficients A_1, A_2, A_3, A_4 evaluated for the three retarder sequence one obtains

$$
\begin{aligned}
2(A_3^2+A_4^2) = {} & 1-[1-\Omega_1][1-\Omega_2][1-\Omega_3] \\
& +[1-\Omega_1]\{\sin\varphi_2 \sin\varphi_3 f_{23}-(1-\cos\varphi_2)(1-\cos\varphi_3)g_{22}g_{33}\} \\
& +[1-\Omega_2]\{\sin\varphi_1 \sin\varphi_3 f_{13}-(1-\cos\varphi_1)(1-\cos\varphi_3)g_{11}g_{33}\} \\
& +[1-\Omega_3]\{\sin\varphi_1 \sin\varphi_2 f_{12}-(1-\cos\varphi_1)(1-\cos\varphi_2)g_{11}g_{22}\} \\
& -\sin\varphi_1 \sin\varphi_2(1-\cos\varphi_3)g_{32}g_{13} \\
& -\sin\varphi_1 \sin\varphi_3(1-\cos\varphi_2)g_{32}g_{12} \\
& -\sin\varphi_2 \sin\varphi_3(1-\cos\varphi_1)g_{32}g_{11} \\
& +(1-\cos\varphi_1)(1-\cos\varphi_2)(1-\cos\varphi_3)g_{11}(1-2f_{22})g_{33} \qquad (28)
\end{aligned}
$$

and

$$
\begin{aligned}
2(A_2A_4-A_1A_3) = {} & [1-\Omega_1][1-\Omega_2](1-\cos\varphi_3)g_{33} \\
& -[1-\Omega_1][1-\Omega_3](1-\cos\varphi_2)g_{22} \\
& +[1-\Omega_2][1-\Omega_3](1-\cos\varphi_1)g_{11} \\
& +[1-\Omega_1]\{\sin\varphi_2 \sin\varphi_3 g_{23}+(1-\cos\varphi_2)(1+\cos\varphi_3)g_{22}\} \\
& +[1-\Omega_2]\{\sin\varphi_1 \sin\varphi_3 g_{13}-(1-\cos\varphi_1)(1+\cos\varphi_3)g_{11}\} \\
& -[1-\Omega_3]\{\sin\varphi_1 \sin\varphi_2 g_{12}+(1-\cos\varphi_1)(1+\cos\varphi_2)g_{11}\} \\
& +(1-\cos\varphi_1)g_{11}\{(1+\cos\varphi_2)(1+\cos\varphi_3)-\sin\varphi_2 \sin\varphi_3 \cos 2\theta_2 \cos 2\theta_3\} \\
& +\sin\varphi_1 \sin\varphi_2\{(1+\cos\varphi_3)g_{12}-(1-\cos\varphi_3)f_{12}g_{33}\}-\sin\varphi_1(1-\cos\varphi_2)\sin\varphi_3(1-f_{22})g_{13} \\
& +(1-\cos\varphi_1)(1-\cos\varphi_2)(1-\cos\varphi_3)g_{11}g_{22}g_{33}\,, \qquad (29)
\end{aligned}
$$

where

$$\Omega_i=(1-\cos\varphi_i)\sin^2 2\theta_i\,, \qquad (30)$$

$$f_{ij}=\sin 2\theta_i \sin 2\theta_j\,, \qquad (31)$$

$$g_{ij}=\sin 2\theta_i \cos 2\theta_j\,. \qquad (32)$$

Equations (27)–(32) completely describe the system with optical elements of arbitrary retardation and orientation. In the case that $\varphi_1,\varphi_2,\varphi_3$ are all small, the power series expansion of Eq. (28) including terms up to fourth order is

$$
\begin{aligned}
4(A_3^2+A_4^2) \approx {} & \{\varphi_1^2 f_{11}+\varphi_2^2 f_{22}+\varphi_3^2 f_{33}+2\varphi_1\varphi_2 f_{12}+2\varphi_1\varphi_3 f_{13}+2\varphi_2\varphi_3 f_{23}\} \\
& -\tfrac{1}{12}\{\varphi_1^4 f_{11}+\varphi_2^4 f_{22}+\varphi_3^4 f_{33}\} \\
& -\tfrac{1}{3}\{\varphi_1\varphi_2(\varphi_1^2+\varphi_2^2)f_{12}+\varphi_1\varphi_3(\varphi_1^2+\varphi_3^2)f_{13}+\varphi_2\varphi_3(\varphi_2^2+\varphi_3^2)f_{23}\} \\
& -\tfrac{1}{2}\{\varphi_1^2\varphi_2^2 f_{12}\cos(2\theta_1-2\theta_2)+\varphi_1^2\varphi_3^2 f_{13}\cos(2\theta_1-2\theta_3)+\varphi_2^2\varphi_3^2 f_{23}\cos(2\theta_2-2\theta_3)\} \\
& -\varphi_1\varphi_2\varphi_3 f_{13}\{\varphi_1\cos(2\theta_1-2\theta_2)+\varphi_2+\varphi_3\cos(2\theta_2-2\theta_3)\}. \qquad (33)
\end{aligned}
$$

The corresponding expression for $4(A_2A_4-A_1A_3)$ is identical except that g_{ij} replaces f_{ij}. The above expressions have been used to derive Eqs. (10), (15), and (24) which are employed in the analysis of the systematic errors in Kerr effect optical retardation measurements. The limiting cases for two or one retarder are obtained by setting one or two of $\varphi_1,\varphi_2,\varphi_3$ to zero.

[1] M. P. Bogaard and B. J. Orr, in *International Review of Science, Physical Chemistry, Molecular Structure and Properties*, edited by A. D. Buckingham (Butterworths, London, 1975), Ser. 2, Vol. 2, p. 149.

[2] A. D. Buckingham, in *Molecular Electro-Optics, Pt. I, Theory and Methods*, edited by C. T. O'Konski (Marcel Dekker, New York, 1976), p. 27.

[3] I. R. Gentle, D. R. Laver, and G. L. D. Ritchie, J. Phys. Chem. **94**, 3434 (1990).

[4] L. L. Boyle, A. D. Buckingham, R. L. Disch, and D. A. Dunmur, J. Chem. Phys. **45**, 1318 (1966).

[5] A. D. Buckingham and H. Sutter, J. Chem. Phys. **64**, 364 (1976).

[6] A. K. Burnham, L. W. Buxton, and W. H. Flygare, J. Chem. Phys. **67**, 4990 (1977).
[7] S. Carusotto, E. Iacopini, E. Polacco, F. Scuri, G. Stefanini, and E. Zavattini, Nuovo Cimento **5D**, 328 (1985); J. Opt. Soc. Am. B **1**, 635 (1984).
[8] I. R. Gentle, D. R. Laver, and G. L. D. Ritchie, J. Phys. Chem. **93**, 3055 (1989).
[9] R. Tammer and W. Huttner, Chem. Phys. **146**, 155 (1990).
[10] D. M. Bishop, Rev. Mod. Phys. **62**, 343 (1990).
[11] A. D. Buckingham and B. J. Orr, Proc. Roy. Soc. London A **305**, 259 (1968).
[12] D. P. Shelton and R. E. Cameron, Rev. Sci. Instrum. **59**, 430 (1988).
[13] R. Piazza, V. Degiorgio, and T. Bellini, Opt. Commun. **58**, 400 (1986).
[14] F. Mendicuti, Rev. Sci. Instrum. **59**, 728 (1988).
[15] R. Guenther, *Modern Optics* (Wiley, New York, 1990).
[16] A. D. Buckingham and R. L. Disch, Proc. Roy. Soc. London A **273**, 275 (1963).
[17] D. P. Shelton, Rev. Sci. Instrum. **63**, 3978 (1992).
[18] S. M. Saltiel, P. D. Yankov, and N. I. Zheludev, Appl. Phys. B **42**, 115 (1987).
[19] E. O. Forster, J. Chem. Phys. **37**, 1021 (1962).
[20] M. Silver, J. Chem. Phys. **42**, 1011 (1965).
[21] Z. Croitoru, in *Progress in Dielectrics*, edited by J. B. Brinks and J. Hart (Academic, New York, 1965), Vol. 6, p. 103.
[22] G. Biere and F. Gaspard, Chem. Phys. Lett. **1**, 706 (1968).
[23] E. J. Hopfinger and J. P. Gosse, Phys. Fluids **14**, 1671 (1971).
[24] J. C. Lacroix, P. Atten, and E. J. Hopfinger, J. Fluid Mech. **69**, 539 (1975).
[25] N. J. Felici and J. C. Lacroix, J. Electrost. **5**, 135 (1978).
[26] E. Kuffel and W. S. Zaengl, *High-Voltage Engineering* (Pergamon, Oxford, 1984).
[27] L. Chaumont, Ann. Phys. **5**, 31 (1916).
[28] E. A. Volkova, V. A. Zamkov, and L. V. Nalbandov, Opt. Spectrosc. **30**, 300 (1971).
[29] G. Arfken, *Mathematical Methods for Physicists* (Academic, New York, 1970).
[30] J. D. Jackson, *Classical Electrodynamics* (Wiley, New York, 1975).
[31] S. D. Fisher, *Complex Variables*, 2nd ed. (Wadsworth and Brooks, Pacific Grove, 1990).
[32] G. Leclerc and L. Sanche, Comput. Phys. **4**, 617 (1990).
[33] E. Ryshkewitch, *Oxide Ceramics* (Academic, New York, 1960).
[34] T. Masaki and K. Kobayashi, in *Advanced Ceramics*, edited by S. Saito (Oxford University Press, Oxford, 1988).
[35] R. C. Weast, ed., *Handbook of Chemistry and Physics*, 68th ed. (CRC, Boca Raton, 1987).
[36] L. H. Johnson, S. R. Raju, and G. R. Sudhakaran, J. Mol. Spectrosc. **89**, 556 (1981).
[37] J.-G. Lahaye, C. Lambeau, A. Fayt, J. Lemaire, F. Herlemont, and M. Lyszyk, Appl. Opt. **24**, 1657 (1985).
[38] B. Scruton and B. H. Blott, J. Phys. E **6**, 472 (1973).
[39] P. Horowitz and W. Hill, *The Art of Electronics* (Cambridge University Press, Cambridge, 1989).
[40] H. G. Jerrard, J. Opt. Soc. Am. **44**, 289 (1954).